CORE
Metadata, citation and similar papers at core.ac.uk
Provided by Tamkang University Institutional Repository



# Effect of pretreatment bias on the nucleation and growth mechanisms of ultrananocrystalline diamond films via bias-enhanced nucleation and growth: An approach to interfacial chemistry analysis via chemical bonding mapping

X. Y. Zhong,[1,a)] Y. C. Chen,[2] N. H. Tai,[2] I. N. Lin,[3] J. M. Hiller,[1] and O. Auciello[1,4]
[1]*Materials Science Division, Argonne National Laboratory, Argonne, Illinois 60439, USA*
[2]*Department of Materials Science and Engineering, National Tsing-Hua University, Hsinchu 300, Taiwan*
[3]*Department of Physics, Tamkang University, Tamsui 251, Taiwan*
[4]*Center for Nanoscale Materials, Argonne National Laboratory, Argonne, Illinois 60439, USA*

(Received 8 September 2008; accepted 6 December 2008; published online 10 February 2009)

The effect of pretreatment bias on the nucleation and growth mechanisms of the ultrananocrystalline diamond (UNCD) films on the Si substrate via bias-enhanced nucleation and bias-enhanced growth (BEN-BEG) was investigated using cross-sectional high-resolution transmission electron microscopy, chemical bonding mapping, and Raman spectroscopy. The mirror-polished substrate surface showed the formation of a triangular profile produced by a dominant physical sputtering mechanism induced by ion bombardment of ions from the hydrogen plasma accelerated toward the substrate due to biasing and a potential hydrogen-induced chemical reaction component before synthesizing the UNCD films. The BEN-BEG UNCD films grown on the Si substrate with biased and unbiased pretreatments in the hydrogen plasma were compared. In the case of the bias-pretreated substrate, the SiC phases were formed at the peaks of the Si surface triangular profile due to the active unsaturated Si bond and the enhanced local electrical field. The UNCD grains grew preferentially at the peaks of the triangular substrate surface profile and rapidly covered the amorphous carbon (*a*-C) and oriented graphite phases formed in the valley of the surface profile. In the case of the substrate with unbiased pretreatment, the SiC phases were formed via the reactions between the hydrocarbon species and the active Si atoms released from the substrate with assistance of the hydrogen plasma. The UNCD grains nucleated on the nucleating sites consisting of the SiC, *a*-C, and graphite phases. Growth mechanisms for the BEN-BEG UNCD films on both Si substrates were proposed to elucidate the different nucleation processes. Applying bias on the Si substrate pretreated in the hydrogen plasma optimized the nucleation sites for growth of UNCD grains, resulting in the low content of the nondiamond phases in UNCD films. © *2009 American Institute of Physics*. [DOI: 10.1063/1.3068366]

## I. INTRODUCTION

Ultrananocrystalline diamond (UNCD) in thin film form is an outstanding candidate material for fabrication of multifunctional devices such as several microelectromechanical systems and nanoelectromechanical systems (MEMS/NEMS) devices that require specific properties as high Young's modulus, low friction coefficient, low surface work of adhesion, high resistance to wear,[1] and integration with dissimilar materials such as piezoelectric oxides to enable piezoactuated diamond-based MEMS/NEMS devices.[2] UNCD films exhibit exceptional mechanical, tribological, electrochemical, and biocompatible properties similar to those of single crystal diamond. One of the key issues in optimizing the performances of UNCD films is providing better seeding layers on various substrates to synthesize UNCD films with their characteristic nanostructure (2–5 nm grains and 0.4 nm grain boundaries), but with higher density, smoother surface, and higher deposition rates than hitherto achieved, using wet chemical seeding with enhanced nucleation layers plus UNCD film growth process.[3] In this respect, recent work demonstrated that bias-enhanced nucleation (BEN) provided a dry plasma-assisted means to producing controllable, high nucleation density to grow diamond thin films on Si substrates.[4,5] However, prior bias-enhanced nucleation and bias-enhanced growth (BEN-BEG) processes using $H_2/CH_4$ chemistries produced nanocrystalline diamond films (30–100 nm grain size) exhibiting larger clusters (cauliflower morphologies), limited surface smoothness, high compressive stress, delamination, and high content of nondiamond phase.[6–8]

Recently, we developed a low-pressure heat-assisted BEN-BEG process to synthesize UNCD films with nanoscale surface roughness, high growth rate, uniform nanosized crystalline diamond grains, and very low content of $sp^2$ bonded carbon atoms, exhibiting promising tribological properties.[9] However, understanding the growth mechanism of BEN-BEG UNCD films on Si substrates is a crucial but difficult task because of the complex nature in the synthesis process. In the previous studies,[10,11] a mechanism involving two complementary stages was proposed to explain the diamond nucleation on Si substrates via the traditional BEN process

[a)]Electronic mail: xzhong@anl.gov.

 © 2009 American Institute of Physics

Downloaded 22 Feb 2010 to 163.13.32.173. Redistribution subject to AIP license or copyright; see http://jap.aip.org/jap/copyright.jsp

with the stages being (a) subplantation of energetic $C^+$ ions from the plasma, accelerated by the bias applied on the substrate, causing formation of a hydrogenated amorphous carbon ($a$-C:$H$) layer on the substrate surface, and (b) diamond nucleation, where the graphitic planes are locally oriented perpendicular to the surface. An alternative mechanism was that a SiC layer might be formed, leading to diamond nucleation because of the reduced lattice mismatch between diamond and SiC compared to diamond and Si.[5,12]

Therefore, it is important to investigate the structure, composition, and bonding of the UNCD/Si interfaces. The atomic structure of specific interfaces can be obtained by high-resolution transmission electron microscopy (HRTEM) studies,[7,10,13,14] whereas energy-filtered transmission electron microscopy (EFTEM) and electron energy-loss spectroscopy (EELS) provide information on the chemical composition and the local electronic structure of interfaces.[15–19] The information can be extracted from the analysis of the energy-loss near-edge structure (ELNES) associated with each ionization edge in the EELS spectrum.[20,21] The ELNES gives information on the density of unoccupied states above the Fermi level that reflect transitions from the highly localized atomic orbitals on single atomic sites. Changes in the bonding character or the valency of atoms can modify the distribution of unoccupied electronic states, which reflects in the shape of the ELNES and/or chemical shifts of the threshold energy of the specific edge. Applying the electron spectroscopic imaging (ESI) technique to a characteristic ELNES of the specific inner shell loss edge, information on the distribution of the corresponding chemical bond can be obtained.[18,22–24] Mayer and Plitzko[18] and Muller *et al.*[22] demonstrated that the distribution of $sp^2$ and $sp^3$ hybridized carbon could be mapped via the presence of the $\pi^*$ and $\sigma^*$ excitations in the C $K$ edge. We extended this method to map the Si–C and Si–Si bonds due to the 3 eV chemical shift in the Si $K$ edge between two bonds.

Here we developed a protocol for preparing cross-sectional samples of the UNCD films on the Si substrate to allow direct mapping of chemical bonding and observation of the atomic arrangement at interfaces. A comprehensive study on the UNCD-substrate interface using HRTEM and chemical bonding mapping was performed to obtain nanoscale information of the nucleation and early stages of the growth process caused by bias pretreatment and BEN-induced silicon morphological changes to substantiate our proposed mechanism for the BEN-BEG of UNCD films on Si surfaces.

## II. EXPERIMENTAL

To investigate effects of pretreatment bias on the BEN-BEG UNCD film growth, the $n$-type Si (100) substrates with biased and unbiased pretreatments were prepared. One was a mirror-polished Si substrate with the native $SiO_2$ layer exposed to hydrogen plasma for 10 min without applying any bias. The other was a Si substrate pretreated in hydrogen plasma under $-350$ V bias for 10 min. Following prior processes in the hydrogen plasma, UNCD films were grown for 25 min on both substrates heated to 1123 K under $-350$ V bias using a $H_2(93\%)/CH_4(7\%)$ plasma produced by 2.2 kW microwave power at 25 mbar pressure in a 2.45 GHz 6 in. IPLAS CYRANNUS microwave plasma chemical vapor deposition system. The overall nucleation and growth process was defined as the BEN-BEG process.

The bonding structure of UNCD films was examined by visible Raman spectroscopy (Renishaw, green 514 nm) performed at room temperature. In order to clearly characterize the interfacial structures between the UNCD films and the Si substrate, cross-sectional TEM samples were prepared in a Zeiss 1540X dual beam focused ion beam (FIB) system. An $Ar^+$ ion gentle milling at grazing incidence was done to remove the FIB-damaged surface layers. The analytical TEM experiments were performed in a field emission transmission electron microscope (Tecnai F20ST), equipped with a post-column energy filter (Gatan) and using a 200 keV electron beam. The dark current and gain variation were corrected while screening the electron beam and uniformly illuminating the charge coupled device without a sample, respectively. The energy dispersion of the EELS spectra was 0.1 eV/pixel. The spectral background of the ionization edge was removed by fitting the pre-edge background with a power law function. The ESI for silicon was acquired from 79 to 115 eV loss with a step width of 3 eV and an energy slit width of 3 eV, while the ESI for carbon was acquired from 263 to 296 eV loss with a step width of 3 eV and an energy slit width of 4 eV. All the ESI series were well aligned to correct the sample drift.

## III. RESULTS AND DISCUSSION

Figure 1(a) shows the HRTEM plain-view image of an UNCD film grown on a Si substrate exposed to a pure hydrogen plasma under bias to remove the native $SiO_2$ layer from the surface, followed by the *in situ* BEN-BEG process. Figure 1(a) clearly reveals a dense UNCD nanograin structure with atomic wide grain boundaries, while diffraction analysis shows no evidence of a graphite phase as indicated by the selected area electron diffraction (SAED) pattern [cf. inset in Fig. 1(a)]. Figure 1(b) shows a HRTEM image of the top surface of a UNCD film grown on a Si substrate pretreated in a pure hydrogen plasma without bias but subjected also to the BEN-BEG process. Figure 1(b) clearly reveals UNCD grains and the grain boundaries consisting of an $a$-C phase and a small amount of graphite phase with its (0001) lattice fringes as marked in the SAED pattern [cf. inset in Fig. 1(b)]. Figures 1(c) and 1(d) show the core-loss EELS spectra and the Raman spectra, respectively, from the UNCD films grown on the Si substrate with biased and unbiased pretreatments. The signal ratio of the carbon $\sigma^*$ to $\pi^*$ peaks in the core-loss EELS spectrum from the UNCD films grown on the bias-pretreated Si substrate was much stronger than that from the UNCD films grown on the Si substrate with unbiased pretreatment after normalized by the integrals of the carbon $\pi^*$ peaks. The EELS analysis demonstrated the lower content of the graphite and $a$-C phases in the UNCD films grown on the bias-pretreated Si substrate as opposed to the films grown on the Si surface exposed to the unbiased pretreatment. The $D$-peak in the Raman spectra from the

Downloaded 22 Feb 2010 to 163.13.32.173. Redistribution subject to AIP license or copyright; see http://jap.aip.org/jap/copyright.jsp

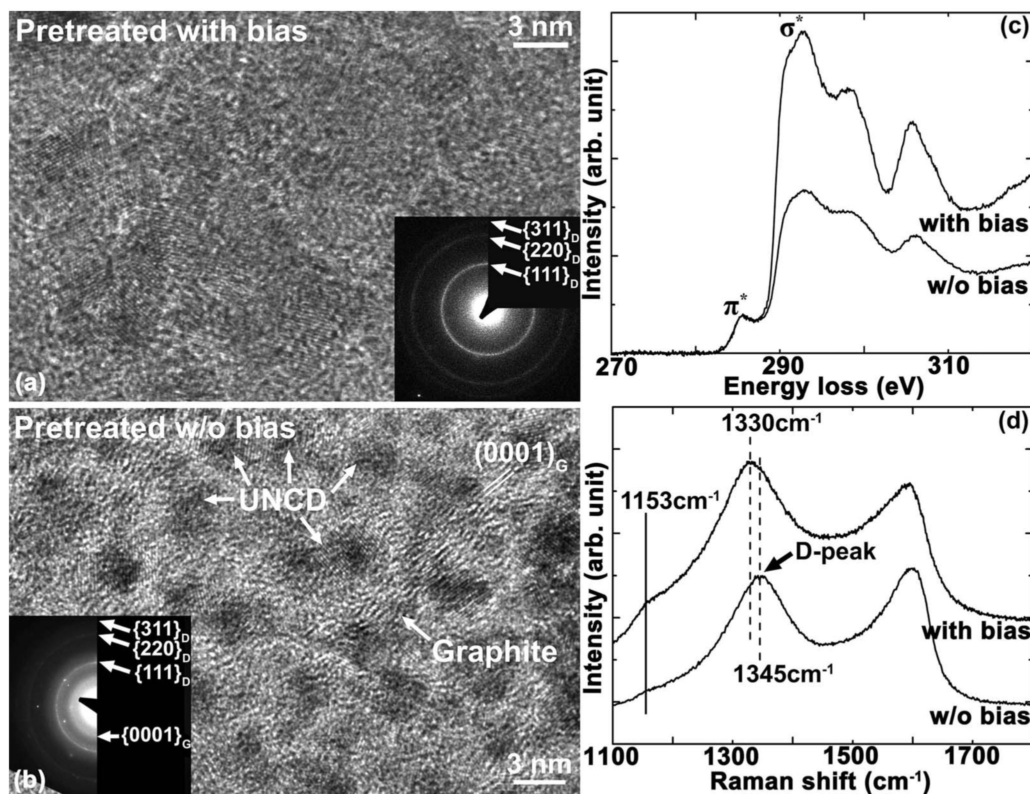


FIG. 1. HRTEM plain-view images of UNCD films grown on the Si substrates with (a) biased and (b) unbiased pretreatments in a pure hydrogen plasma, followed by the BEN-BEG process, and their corresponding (c) core-loss EELS spectra and (d) the Raman spectra showing the lower content of the nondiamond phases in the UNCD films grown on the bias-pretreated Si substrate, as opposed to films grown on unbiased pretreatment substrates.

UNCD films grown on the bias-pretreated Si substrate shifted 15 eV to the lower wave number with respect to that from the UNCD films grown on the Si substrate with unbiased pretreatment, indicating the lower fraction of the $sp^2$-bonded carbon in the UNCD films on the bias-pretreated Si substrate. Additionally, the 1153 $cm^{-1}$ peak taken as a criterion for a nanocrystalline diamond phase[25] from the UNCD film grown on the bias-pretreated Si substrate is more intense than that from the UNCD film grown on the Si substrate with unbiased pretreatment. The experimental results show that the content of the nondiamond phases in the UNCD film grown on the bias-pretreated Si substrate is much less than for the UNCD film grown on the Si substrate with unbiased pretreatment.

Cross-sectional HRTEM studies were performed to distinguish the differences in the nucleation sites between the biased (cf. Figs. 2 and 3) and unbiased (cf. Figs. 4 and 5) substrate pretreatments. Figures 2(a) and 2(b) show the typical cross-sectional low-magnification TEM and HRTEM images, respectively, of a BEN-BEG UNCD film on the bias-pretreated Si substrate, clearly revealing the UNCD grains, the etched Si surface, and the UNCD/Si interfacial layer. The formation of the observed triangular profile on the surface of the Si substrate with a peak-to-valley roughness of about 15 nm can be attributed to the preferential etching of the Si substrate along the (100) direction induced by the ion bombardment during the 10 min of hydrogen plasma pretreatment. The same triangular Si surface morphology was observed previously on a silicon surface during a diamond BEN process.[10] However, no detailed explanation was given regarding its origin. We believe that hydrogen ion bombardment results in preferential etching of the Si surface along the (100) crystallographic direction, which etches faster than the (111) direction due to a higher physical sputtering rate of the (100) direction, as shown in prior work on physical sputtering of Si surface.[26] The physical dominated etching process may be enhanced by chemical reactions of hydrogen atoms with Si atoms on the surface of the Si substrate. This physical dominated mechanism for etching of the Si surface results in the triangular Si interface profile defined by the (111) planes.[26] The boundary of the UNCD films, as shown by the white solid line in Fig. 2(b), reveals a preferential nucleation of UNCD grains at the peaks of the Si surface triangular profile, while *a*-C/graphitic phases appear to nucleate at the valleys of the Si surface profile. The UNCD grains nucleated at the peaks of the Si surface triangular profile rapidly extend sidewise covering the *a*-C and graphite phases grown in the valleys. Figures 2(c) and 2(d) show the enlarged HRTEM images of the valley area [marked as I in Fig. 2(b)] and the peak area [marked as II in Fig. 2(b)], respectively. The interface layer in the valley of the Si substrate consisted mainly of the *a*-C phase and the graphite phase with its (0001) planes approximately perpendicular to the Si (100) surface [cf. Fig. 2(c)]. By contrast, SiC grains were found in an interface layer about 5 nm thick between the UNCD grains and the peak of the Si triangular surface profile [cf. Fig. 2(d)].

To further confirm the HRTEM observation at interfaces between the UNCD films and the rough Si substrate, chemical bonding information was acquired via ESI of silicon and

Downloaded 22 Feb 2010 to 163.13.32.173. Redistribution subject to AIP license or copyright; see http://jap.aip.org/jap/copyright.jsp

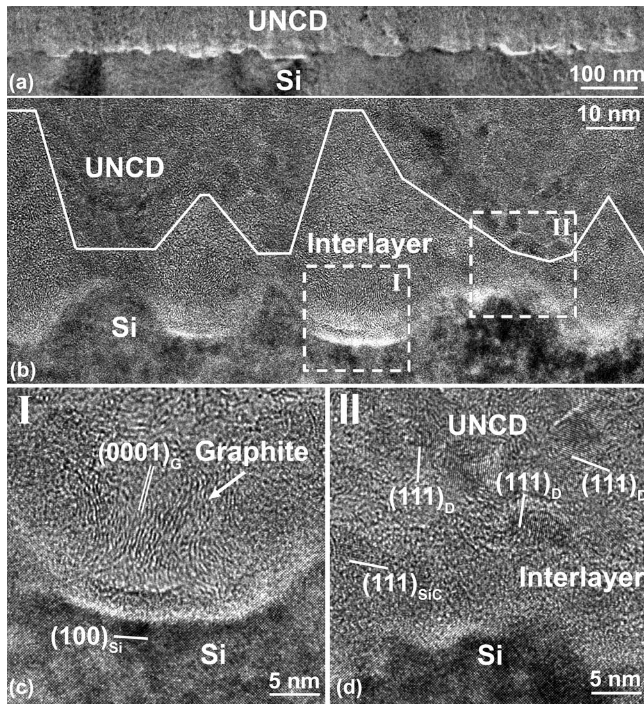


FIG. 2. Typical cross-sectional (a) low-magnification TEM and (b) HRTEM images of a BEN-BEG UNCD film grown on the bias-pretreated Si substrate showing UNCD grains, the UNCD-Si interface layer, and the Si substrate. The white solid line in (b) shows the boundary between the UNCD and the interface layer, clearly demonstrating preferential nucleation of UNCD grains at the peaks of the Si triangular surface profile. The enlarged HRTEM images of (c) the valley area and (d) the peak area correspond to the dashed squares marked as I and II, respectively, in (b). The interface layer in the valleys of the triangular Si surface profile is rich in the *a*-C and graphite phases. By contrast, some SiC grains are found in about 5 nm thick interlayer between the UNCD grains and the peaks of the Si substrate.

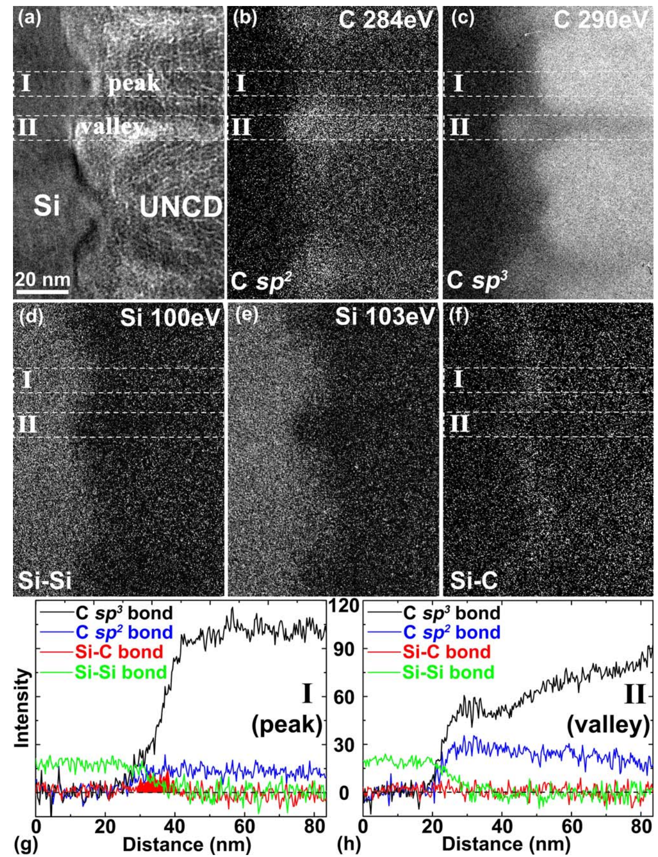


FIG. 3. (Color online) (a) TEM image of the UNCD films on the bias-pretreated Si substrate and the corresponding series of chemical bonding maps obtained from (b) the carbon $\pi^*$ peak for carbon $sp^2$ bond, (c) the carbon $\sigma^*$ peak for carbon $sp^3$ bond, (d) the Si $K$ edge at 100 eV energy loss for Si–Si bond, and (e) the Si $K$ edge at 103 eV energy loss for Si–C and Si–Si bonds. (f) Difference in the EFTEM images taken at 100 and 103 eV energy loss clearly distinguishes the Si–C bond from the Si–Si bond. The profiles of the dashed rectangles in (g) the peak area and (h) the valley area in the chemical maps from the Si–Si bond, the Si–C bond, and the C $sp^2$ and $sp^3$ bonds were taken as a line scan along the axis perpendicular to the Si surface, clearly revealing an interface layer containing SiC grains at the peaks and an interface layer rich in the *a*-C and graphite phases in the valleys.

carbon. A series of chemical bonding maps was obtained from the carbon $\pi^*$ peak at 284 eV for carbon $sp^2$ bond [cf. Fig. 3(b)], the carbon $\sigma^*$ peak at 290 eV for carbon $sp^3$ bond [cf. Fig. 3(c)], the Si $K$ edge at 100 eV for Si–Si bond [cf. Fig. 3(d)], and the Si $K$ edge at 103 eV for both Si–C bond and Si–Si bond [cf. Fig. 3(f)], corresponding to TEM images of the UNCD films on the bias-pretreated substrate [cf. Fig. 3(a)]. The high-intensity area in the carbon $sp^2$ bonding map manifested the *a*-C and graphite phases with the substantial $\pi$-bond in the valleys of the Si triangular surface profile [cf. Fig. 3(b)], while the high-intensity area in the carbon $sp^3$ bonding map further demonstrated that UNCD grains were preferentially nucleated at the peaks of the Si triangular surface profile [cf. Fig. 3(c)]. Figure 3(e) shows the difference in the EFTEM images obtained at 100 and 103 eV energy loss, clearly distinguishing the Si–C bond from the Si–Si bond since the threshold energies of the Si $K$ edge for the Si–Si and Si–C bonds are 100 and 103 eV, respectively. The layer with low but recognizable Si–C bonding signals between the UNCD grains and the peaks of the Si triangular surface profile corresponded to the interfacial layer consisting of the SiC grains in the HRTEM images. To better plot the chemical bonding information, the profiles of the dashed rectangles in the peak area [marked as I, cf. Fig. 3(g)] and the valley area [marked as II, cf. Fig. 3(f)] in the chemical maps from the Si–Si bond, the Si–C bond, and the C $sp^2$ and $sp^3$ bonds were taken as a line scan along the axis perpendicular to the Si surface. In the area around the peak of the Si surface triangular profile, the Si–C bonding signals filled with the red area were detected at interfaces between the UNCD films and the Si substrate, while the Si–Si bonding signals were only remarkable within the Si substrate. Above the Si–C bonding layer, the C $sp^2$ and $sp^3$ bonding signals rapidly reached saturation, implying the formation of the UNCD grains. In the area around the valley of the Si surface triangular profile, the C $sp^2$ bonding signals met the maximum at interfaces between the UNCD films and the Si substrate and decreased with the film thickness, while the C $sp^3$ bonding signals increased with the film thickness, indicating that the graphite and *a*-C phases formed in the valleys were gradually covered by the UNCD grains. No Si–C bonding signal was detected in the valleys, while the Si–Si bonding signal was highlighted within the Si substrate. Apparently, the nucleation sites on the bias-pretreated substrate strongly depended on the local substrate morphology such as peaks and valleys of the observed Si surface triangular profile.

Downloaded 22 Feb 2010 to 163.13.32.173. Redistribution subject to AIP license or copyright; see http://jap.aip.org/jap/copyright.jsp

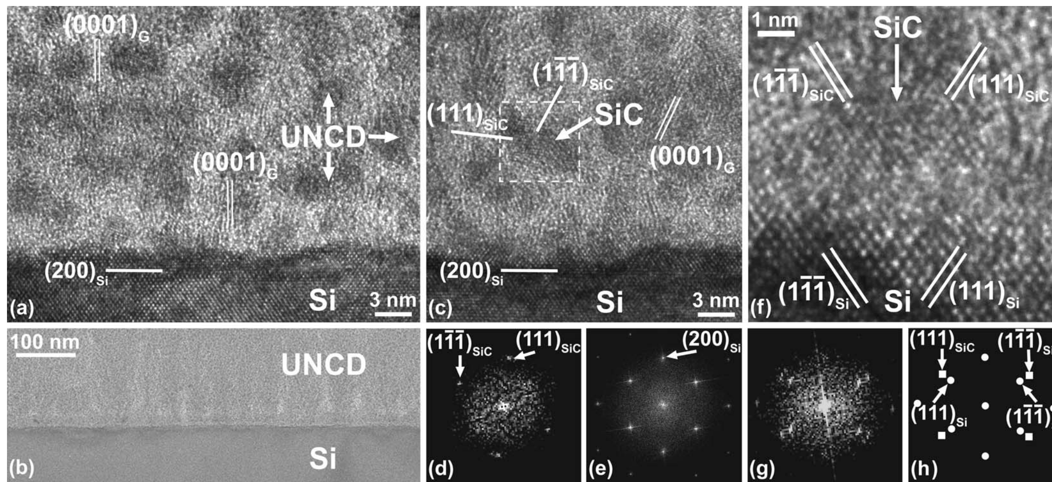


FIG. 4. Typical cross-sectional (a) high-resolution and (b) low-magnification TEM images of the BEN-BEG UNCD films on the Si substrate with unbiased pretreatment clearly reveal the graphite phase, the UNCD grains, and the Si substrate. (c) HRTEM image of the SiC grain (white dashed square) embedded in the seeding layer consisting of the *a*-C and graphite phases and the corresponding optical diffractograms from (d) the SiC grain and (e) the Si substrate. (f) HRTEM image of the SiC grain grown epitaxially on the Si substrate and (g) its corresponding optical diffractograms. (h) Schematic clearly showing the epitaxial orientation relationship SiC(100)[01$\bar{1}$]‖Si(100)[01$\bar{1}$].

For comparison, the nucleation sites on the Si substrate with unbiased pretreatment were investigated with the same method used to study the UNCD film on the bias-pretreated Si substrate. Figures 4(a) and 4(b) show the typical cross-sectional high-resolution and low-magnification TEM images, respectively, of the BEN-BEG UNCD films on the substrate with unbiased pretreatment, clearly revealing the Si substrate, the UNCD grains with random orientations, and the graphite phase with its (0001) plane. There was no oxygen detected at interfaces between the Si substrate and the UNCD films. The roughness of the Si substrate with unbiased pretreatments was only a few atomic layers after BEN process. The graphite at interfaces grew preferentially perpendicular to the Si surface. Figure 4(c) shows that the SiC grain selected by the white dashed square is embedded in the seeding layer mixed with the *a*-C and graphite phases. Based on the optical diffractograms from the selected grain [cf. Fig. 4(d)] and the Si substrate [cf. Fig. 4(e)], it was calculated that the grain could be identified as the cubic SiC phase oriented along its [01$\bar{1}$] zone axis. Figure 4(f) shows that another SiC grain grew epitaxially on the Si substrate. The optical diffractogram from both the grain and the Si substrate and its schematic diagram are shown in Figs. 4(g) and 4(h), respectively, clearly illustrating the epitaxial orientation relationship SiC(100)[01$\bar{1}$]‖Si(100)[01$\bar{1}$]. The seeding layer consisting of the *a*-C, graphite, and SiC phases provided the nucleation sites in the initial stage of the UNCD growth on the Si substrate with unbiased pretreatment.

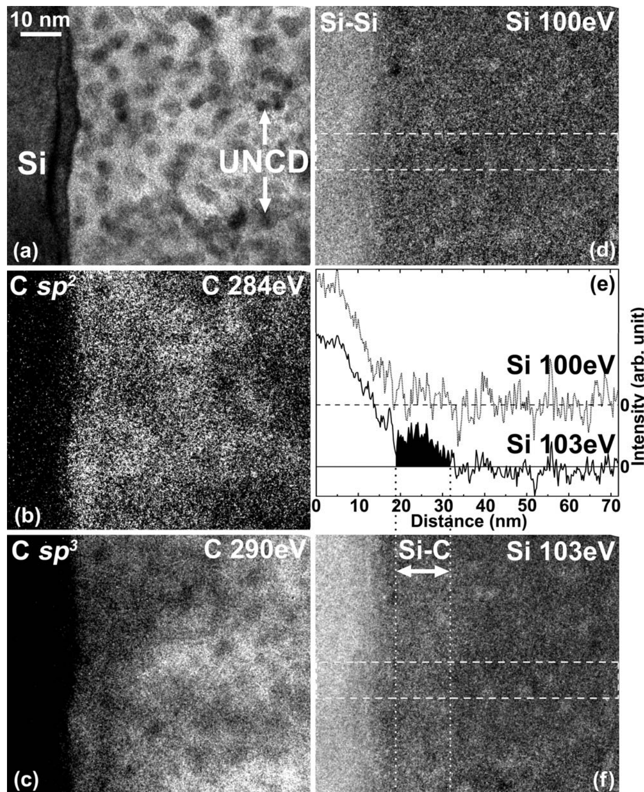


FIG. 5. (a) TEM image of the UNCD films on the substrate with unbiased pretreatment and the corresponding series of chemical bonding maps obtained from (b) the carbon $\pi^*$ peak for carbon $sp^2$ bond, (c) the carbon $\sigma^*$ peak for carbon $sp^3$ bond, (d) the Si *K* edge at 100 eV energy loss for Si–Si bond, and the (f) Si *K* edge at 103 eV energy loss for Si–C and Si–Si bonds. (e) Profiles of the dashed rectangle in the EFTEM images at 100 and 103 eV energy loss taken as a line scan along the axis vertical to the Si surface clearly reveal that the remarkable Si signals above the Si substrate correspond to the 13 nm thick dotted layer containing the SiC phase.

Figure 5 shows a series of chemical bonding maps and the corresponding TEM image recorded from the interfaces between the UNCD films, grown with unbiased pretreatment, and the Si substrate, revealing the chemical information in the seeding layer. The high-intensity area in the carbon $sp^2$ bonding map indicates that the seeding layer above the Si substrate consists of a large amount of the graphite and *a*-C phases [cf. Fig. 5(b)], while the high-intensity area in the carbon $sp^3$ bonding map reveals that the UNCD grains above the seeding layer are denser than those embedded in the seeding layer [cf. Fig. 5(c)]. The Si–Si bonding map from the EFTEM image at 100 eV energy loss reveal that no Si signal is detected above the Si substrate [cf. Fig. 5(d)]. However,

Downloaded 22 Feb 2010 to 163.13.32.173. Redistribution subject to AIP license or copyright; see http://jap.aip.org/jap/copyright.jsp

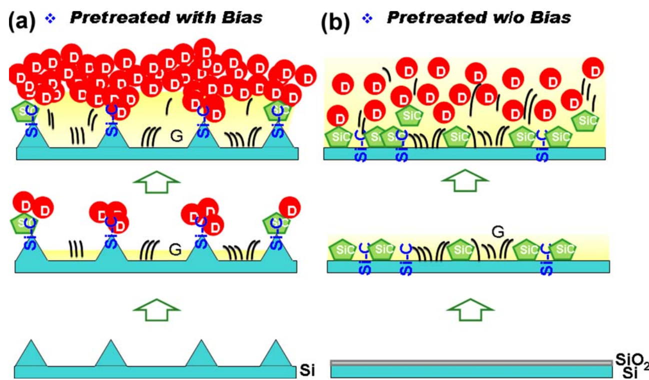


FIG. 6. (Color online) Schematic of the growth mechanisms of the UNCD films on the Si substrates with (a) biased and (b) unbiased pretreatments in the hydrogen plasma.

there is an approximately 13 nm thick dotted layer above the Si substrate with the low but detectable Si signals in the EFTEM image at 103 eV energy loss [cf. Fig. 5(f)], indicating the formation of the SiC phase in the seeding layer. To illustrate the difference in the Si signals from the EFTEM images between 100 and 103 eV energy loss, the profiles of the dashed rectangle in both images were taken as a line scan along the axis perpendicular to the Si surface [cf. Fig. 5(e)]. The remarkable intensity filled with the black area in the line-scan profile from the EFTEM image at 103 eV energy loss corresponds to the 13 nm thick dotted layer containing the SiC phase. It was confirmed that the seeding layer on the Si substrate with unbiased pretreatment was composed of the *a*-C, graphite, and SiC phases in the nucleation stage of the BEN process.

Apparently, substrates with different pretreatments induced different nucleation and growth processes of UNCD grains in the nucleation and crystal growth stages, respectively. Schematic diagrams for the growth mechanisms of the UNCD films on the substrates with biased and unbiased pretreatments are shown in Figs. 6(a) and 6(b), respectively. In the case of the UNCD films grown on the bias-pretreated Si substrate, the nucleation sites depended strongly on the substrate surface morphology. The interface layer in the valleys of the Si triangular surface profile was rich in graphite and *a*-C phases, while the interface layer at the Si peaks contained SiC grains. Two reasons were proposed to explain the formation of the SiC phase. One was the active Si atoms with unsaturated bonding at the peaks of the substrate after etching by hydrogen plasma. The other was the enhanced electrical field due to the high charge concentration at the peaks of the Si surface triangular profile when applying bias, attracting the charged hydrocarbon species in the plasma and resulting in the preferential nucleation of UNCD grains at the peaks. To verify our hypothesis, a series of the UNCD films were synthesized under different biases from $-300$ to $-375$ V with a step of 25 V. It was confirmed that the UNCD grains were nucleated earlier under the higher bias. Additionally, the enhanced electrical field at the peaks of the Si substrate may accelerate the growth of UNCD grains since the growth rate ($\sim$12 nm/min) of UNCD films on the bias-pretreated Si substrate was higher than the growth rate ($\sim$8.4 nm/min) of UNCD films on the Si substrate with unbiased pretreatment for 25 min growth. Diamond grains were more easily formed on itself than on nondiamond phases, so the UNCD grains at the peaks grow rapidly sidewise covering the *a*-C and graphite phases in the valley, minimizing the influence of the nucleation sites of the graphite phases on the subsequent growth process of the UNCD grains. Therefore, there were only a small amount of the nondiamond phases in the UNCD films in the stage of the grain growth. The proposed growth mechanisms of the UNCD films on the bias-pretreated substrate included several concurrent steps [cf. Fig. 6(a)]: (1) silicon etching and formation of silicon (111) oriented triangular facets produced by ion bombardment during the initial hydrogen plasma cleaning process due to preferential etching of the (100) direction, potentially enhanced by chemical reactions between hydrogen and Si atoms, (2) formation of the *a*-C and oriented graphite phases in the valleys of the Si substrate and formation of the SiC phase at the peaks of the Si substrate, (3) preferential nucleation of $sp^3$ diamond clusters on the Si–C bonding phase, and (4) nanodiamond growth from $sp^3$ nanodiamond regions nucleated at the peaks of the Si surface triangular profile.

In the case of the UNCD films on the Si substrate with unbiased pretreatment, the $SiO_2$ layer on the Si substrate appeared to play an important role in generating the SiC grains as the nucleation sites of the UNCD growth. The active Si atoms could be generated from the reduction in the $SiO_2$ layer under the assistance of hydrogen atoms. The SiC grains were formed via reaction between the hydrocarbon species and the active Si atoms. Some SiC grains grew epitaxially on the Si substrate, while others were embedded in the 13 nm thick layer above the Si substrate. Additionally, there were a large amount of the *a*-C and graphite phases on the Si substrate. The UNCD film nucleated on the seeding layer consisting of SiC, *a*-C, and graphite phases. It was inevitable that the mixture of UNCD grains and nondiamond phases was formed by the energetic hydrocarbon species nucleated at the different nucleation sites, resulting in more nondiamond phases in the UNCD films grown on the Si substrate with unbiased pretreatment. The proposed growth mechanisms of the UNCD films on the substrate with unbiased pretreatment followed several concomitant steps [cf. Fig. 6(b)]: (1) reduction in the amorphous $SiO_2$ layer on the Si surface assisted by the impact of hydrogen atoms from the plasma, (2) formation of the SiC phase near the Si substrate via the reaction between Si atoms released from the substrate and hydrocarbon species from the plasma, (3) formation of the hydrogenated $sp^2$ carbon coordinated oriented phases, (4) precipitation of $sp^3$ diamond clusters in the matrix of the SiC, *a*-C, and graphite phases, and (5) nanodiamond growth enhanced by energetic species bombardment at the diamond/hydrogenated carbon interface.

## IV. CONCLUSION

In summary, the substrate-induced effects on the nucleation and growth of the BEN-BEG UNCD films were investigated via cross-sectional HRTEM, chemical bonding mapping, and Raman spectroscopy. The mirror-polished substrate

Downloaded 22 Feb 2010 to 163.13.32.173. Redistribution subject to AIP license or copyright; see http://jap.aip.org/jap/copyright.jsp

surface showed the formation of a triangular profile produced by a dominant physical sputtering process induced by ion bombardment of ions from the hydrogen plasma accelerated toward the substrate due to biasing, potentially enhanced by chemical reaction between H and Si atoms on the Si surface, before growing the UNCD films. The BEN-BEG UNCD films grown on the Si substrate with biased and unbiased pretreatments were compared. In the case of the bias-pretreated substrate, SiC phases were formed at the peaks of the Si surface triangular profile due to chemical bonding between C atoms from the plasma and active unsaturated Si bonds, enhanced by the local electrical field at the Si tip of the surface topography. The UNCD grains grew preferentially at the peaks of the triangular substrate surface profile and rapidly covered the *a*-C and oriented graphite phases formed in the valley of the surface profile. In the case of the substrate with unbiased pretreatment, the SiC phases were formed via the reactions between the C species from the plasma and Si atoms freed from their bonding to $O_2$, assisted by hydrogen atom bombardment of the $SiO_2$ surface. The UNCD grains nucleated on the nucleating sites including the SiC, *a*-C, and graphite phases. Growth mechanisms for the BEN-BEG UNCD films on both Si substrates were proposed to elucidate the different nucleation process, resulting in the lower content of the nondiamond phases in UNCD films grown on the bias-pretreated substrate compared to that grown on the substrate with unbiased pretreatment.

We have demonstrated that cross-sectional HRTEM imaging in conjunction with chemical bonding mapping analysis is a powerful tool for studying the interfacial chemistry of UNCD films on the Si substrate and could apply also to studies on other diamond films grown on Si and other surfaces. The use of the ELNES technique enables obtaining specific chemical bonding information for specific atoms. Increased knowledge on atomic structure and interfacial chemistry at the UNCD/Si interfaces may provide information useful for understanding the growth mechanisms of the BEN-BEG UNCD film, controlling the film structure via the synthesis conditions, and optimizing performance of UNCD films with desired mechanical and tribological properties for MEMS/NEMS devices.

## ACKNOWLEDGMENTS

The authors acknowledge the support of the U.S. Department of Energy, BES-Materials Sciences under Contract No. 58931, both for work in the Materials Science Division and the new Center for Nanoscale Materials under Contract No. DE-AC02-06CH11357. The authors are grateful to Dr. Bernd Kabius of Argonne National Laboratory for the contribution to this paper. R.W.C. acknowledges the support from the Air Force Office of Scientific Research under Contract No. FA9550-05-1-0204. Electron microscopy experiments were carried out at the Electron Microscopy Center for Materials Research at Argonne National Laboratory, a U.S. Department of Energy Office of Science Laboratory operated under Contract No. DE-AC02-06CH11357 by UChicago Argonne, LLC.

[1]O. Auciello, J. Birrell, J. A. Carlisle, J. E. Gerbi, X. C. Xiao, B. Peng, and H. D. Espinosa, J. Phys.: Condens. Matter **16**, R539 (2004).
[2]S. Srinivasan, J. Hiller, B. Kabius, and O. Auciello, Appl. Phys. Lett. **90**, 134101 (2007).
[3]N. N. Naguib, J. W. Elam, J. Birrell, J. Wang, D. S. Grierson, B. Kabius, J. M. Hiller, A. V. Sumant, R. W. Carpick, O. Auciello, and J. A. Carlisle, Chem. Phys. Lett. **430**, 345 (2006).
[4]J. Gerber, S. Sattel, H. Ehrhardt, J. Robertson, P. Wurzinger, and P. Pongratz, J. Appl. Phys. **79**, 4388 (1996).
[5]B. R. Stoner, G.-H. Ma, S. D. Wolter, and J. T. Glass, Phys. Rev. B **45**, 11067 (1992).
[6]T. Sharda, M. Umeno, T. Soga, and T. Jimbo, J. Appl. Phys. **89**, 4874 (2001).
[7]Y. Lifshitz, X. M. Meng, S. T. Lee, R. Akhveldiany, and A. Hoffman, Phys. Rev. Lett. **93**, 056101 (2004).
[8]Y. C. Lee, S. J. Lin, C. T. Chia, H. F. Cheng, and I. N. Lin, Diamond Relat. Mater. **14**, 296 (2005).
[9]Y. C. Chen, X. Y. Zhong, A. Konicek, D. S. Grierson, N. H. Tai, I. N. Lin, B. Kabius, J. M. Hiller, A. V. Sumant, R. W. Carpick, and O. Auciello, Appl. Phys. Lett. **92**, 133113 (2008).
[10]S. T. Lee, H. Y. Peng, X. T. Zhou, N. Wang, C. S. Lee, I. Bello, and Y. Lifshitz, Science **287**, 104 (2000).
[11]W. Lambrecht, C. H. Lee, B. Segall, J. C. Angus, Z. Li, and M. Sunkara, Nature (London) **364**, 607 (1993).
[12]D. N. Belton, S. J. Harris, S. J. Schmeig, A. M. Weiner, and T. A. Perry, Appl. Phys. Lett. **54**, 416 (1989).
[13]J. K. Yan and L. Chang, Nanotechnology **17**, 5544 (2006).
[14]X. Y. Zhong, J. Zhu, and J. Y. Liu, J. Catal. **236**, 9 (2005).
[15]R. F. Egerton, *Electron Energy-Loss Spectroscopy in the Electron Microscope*, 2nd ed. (Plenum, New York, 1996).
[16]X. Y. Zhong, J. Zhu, A. H. Zhang, and S. C. Mou, Appl. Phys. Lett. **89**, 151912 (2006).
[17]V. J. Keast, A. J. Scott, R. Brydson, D. B. Williams, and J. Bruley, J. Microsc. **203**, 135 (2001).
[18]J. Mayer and J. M. Plitzko, J. Microsc. **183**, 2 (1996).
[19]X. Y. Zhong, J. Zhu, and A. H. Zhang, Intermetallics **15**, 495 (2007).
[20]U. Golla-Schindler, G. Benner, and A. Putnis, Ultramicroscopy **96**, 573 (2003).
[21]M. L. Cui, J. Zhu, X. Y. Zhong, Y. G. Zhao, and X. F. Duan, Appl. Phys. Lett. **85**, 1698 (2004).
[22]D. A. Muller, Y. J. Tzou, R. Raj, and J. Silcox, Nature (London) **366**, 725 (1993).
[23]U. Golla and A. Putnis, Phys. Chem. Miner. **28**, 119 (2001).
[24]R. D. Leapman, J. Microsc. **210**, 5 (2003).
[25]J. Birrell, J. E. Gerbi, O. Auciello, J. M. Gibson, J. Johnson, and J. A. Carlisle, Diamond Relat. Mater. **14**, 86 (2005).
[26]O. Auciello and R. Kelly, *Ion Bombardment Modification of Surfaces: Fundamentals and Applications* (Elsevier, New York, 1984).

Downloaded 22 Feb 2010 to 163.13.32.173. Redistribution subject to AIP license or copyright; see http://jap.aip.org/jap/copyright.jsp